RESEARCH ARTICLE

NANO · MICRO small
www.small-journal.com

Biochemical Pathways for n-Type Doping: An Electron Transfer Relay from Saccharide to Organic Semiconductors

Takuma Ohashi, Masaki Ishii, Jun Takeya, Katsuhiko Ariga, and Yu Yamashita**

Solution processing of organic semiconductors provides a facile way to fabricate electrically doped thin films, which opens opportunities for advancing printed electronics. However, this approach is limited due to the instability of dopants and doped organic semiconductors, particularly for n-type ones. In this study, n-type doping of an organic semiconducting polymer is achieved using aqueous doping solutions in air, a condition under which n-type chemical doping had not previously been demonstrated. Polymeric semiconductor thin films are immersed in aqueous doping solutions, which contained the saccharide fructose, redox bio-mediator flavin nucleotide (FMN), and bulky molecular cations. In this process, electrons are transferred from fructose to FMN and then from FMN to organic semiconductor thin films. The introduced electrons are compensated by the incorporation of bulky molecular cations into the thin films. Successful n-type doping is confirmed by absorption, conductivity, and photoelectron spectroscopy measurements. The density of states of the polymer is filled up to −3.8 eV versus vacuum, beyond the conventionally anticipated limit of ambient stability. This breakthrough is rooted in the combined effects of solution pH, mediator-assisted use of fructose, and choice of dopant cation. In addition, n-type doping using biomolecules may shed light on new connections between electronic materials and biomolecules for energy storage, transfer, and conversion.

1. Introduction

Organic semiconductors feature solution processability and electronic properties that are tunable by molecular design,[1,2] making them candidate materials for printed electronics. Recently, chemical doping of organic semiconductors has been employed to improve the performances of photovoltaic cells,[3,4] thermoelectric generators,[5–8] transistors,[9–12] and diodes.[13,14] The doping levels of organic semiconductors reach 10^{21} cm^{-3} for both p-type and n-type,[15–19] which highlights their advantages over other solution-processed semiconductors including oxides and halide perovskites.[20] Ion-exchange doping[15] has enabled the incorporation of stable dopant ions, significantly improving both doping efficiency and environmental stability. Recently, p-type chemical doping of organic semiconductors was demonstrated using aqueous solutions in air, where the use of proton-coupled electron transfer (PCET) reactions offered substantial improvements in both scalability and process control.[21] Together with its n-type counterpart—aqueous solution-based doping in air—this advancement marks a promising step toward the next paradigm in solution-processed organic semiconductors.

To achieve reliable chemical doping, it is critical to suppress undesirable redox reactions with water and/or oxygen. For ambient p-type doping, the reactivity of water is suppressed under low-pH conditions,[21] highlighting the advantage of using pH-controlled aqueous doping solutions. For n-type doping, in addition to the possible reactions with water, reactions with oxygen in air must be addressed. Efficient n-type doping requires that the ionization potential (IP) of the reducing agent be close to or smaller than the electron affinity (EA) of the semiconductor.[22] Given that typical electron-transporting organic semiconductors have EAs around 4.0 eV, strong reducing agents are needed—agents that are generally susceptible to oxidation by oxygen under ambient conditions.[13] Although semiconductors with EA larger than 4.0 eV have been developed,[23,24] materials with relatively small EAs remain important for key applications such as photovoltaic cells, light-emitting diodes, and electron injection layers. To achieve strong and stable n-type chemical doping, various material and process strategies have been investigated, including dimeric dopants,[25]

T. Ohashi, M. Ishii, J. Takeya, K. Ariga, Y. Yamashita
Research Center for Materials Nanoarchitectonics (MANA)
National Institute for Materials Science (NIMS)
1-1 Namiki, Tsukuba, Ibaraki 305-0044, Japan
E-mail: 7221701@alumni.tus.ac.jp; yamashita.yu@nims.go.jp
T. Ohashi, M. Ishii, K. Ariga
Graduate School of Science and Technology
Tokyo University of Science
2641 Yamazaki, Noda, Chiba 278-8510, Japan
J. Takeya, K. Ariga, Y. Yamashita
Department of Advanced Materials Science
Graduate School of Frontier Sciences
The University of Tokyo
5-1-5 Kashiwanoha, Kashiwa, Chiba 277-8561, Japan

The ORCID identification number(s) for the author(s) of this article can be found under https://doi.org/10.1002/smll.202509278

DOI: 10.1002/smll.202509278

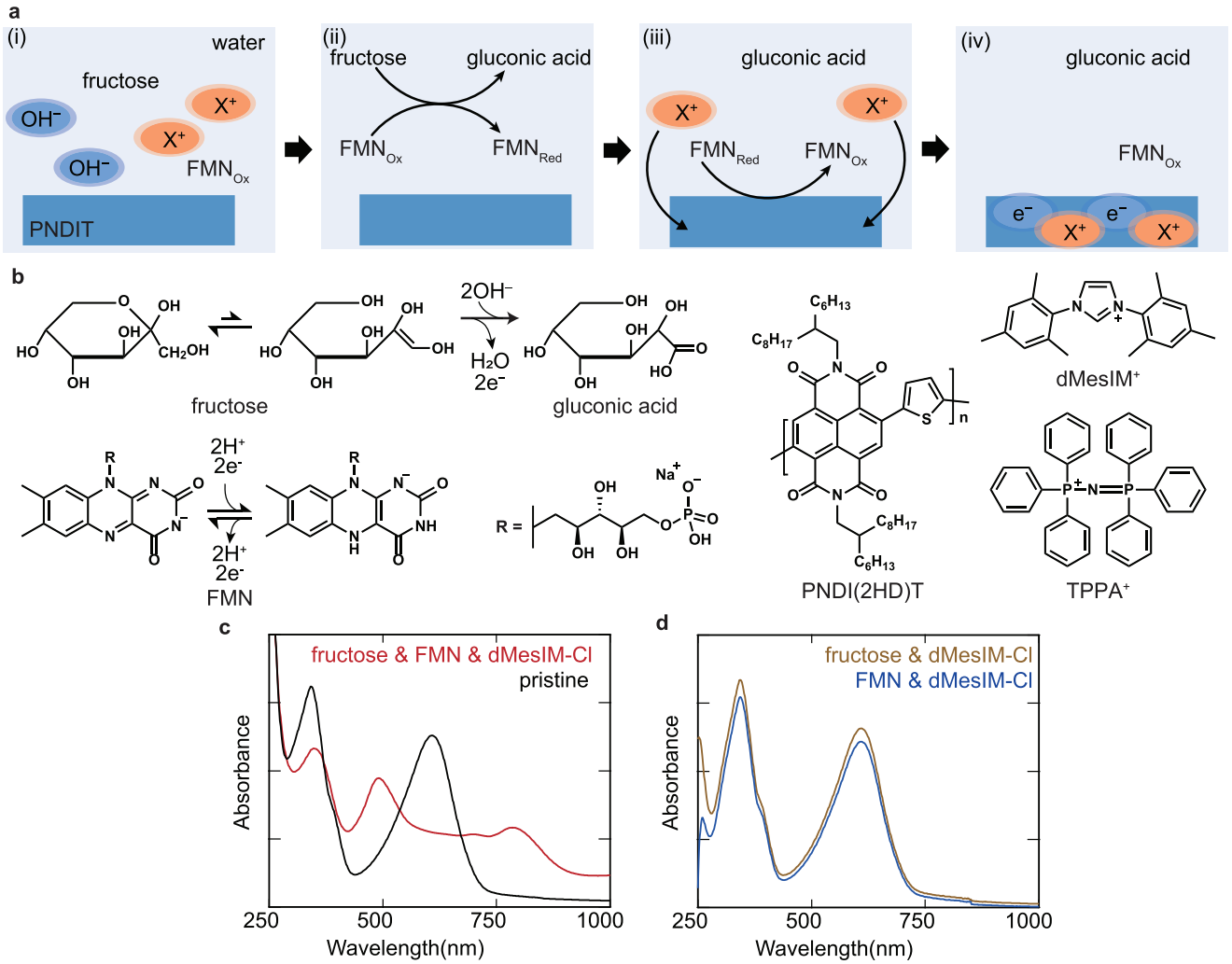

Figure 1. N-type chemical doping under ambient conditions. a) Schematic illustrations of the model of the chemical doping process b) The chemical structures of the employed materials together with schematic illustrations of their possible redox reactions. c,d) UV–Vis spectra of the pristine and treated PNDI(2HD)T thin films. The compounds dissolved in the treatment solutions are denoted as legends. For the red plot, fructose, FMN, and dMesIM-Cl were dissolved in an aqueous pH buffer containing 9vol% acetonitrile.

catalytic doping,[26] and ion-exchange doping.[17,18] However, to the best of our knowledge, efficient n-type chemical doping of organic semiconductors in air has yet to be demonstrated.

While most strongly reducing agents are unstable in air, some biomolecules simultaneously show reducing power and stability. One such example is fructose, a common saccharide found in food. The ambient stability of fructose is due to its slow redox kinetics, where only the enediol form of fructose, which is present at a ratio of 0.4%, contributes to the redox reactions.[27] However, such slow redox kinetics are expected to hinder the efficient electron transfer to other materials, including organic semiconductors. Thus, it is unclear whether such a stable biomolecular energy source can be employed for n-type doping, in which electrons from biomolecules must be transferred to and stored in semiconductors.

In this study, we report n-type chemical doping of organic semiconductors in air using aqueous solutions (**Figure 1a**). To achieve a high reducing power and ambient stability of the reducing agents, we employed a combination of fructose and a redox mediator, flavin mononucleotide (FMN). Electron-transfer reactions occurred from fructose to FMN and then from FMN to semiconductors in our system, which resulted in efficient n-type doping of the semiconductors. The electrons in the semiconductors were compensated by bulky molecular cations, which were selected to improve carrier transport properties and stability. UV–Vis, conductivity, and X-ray photoelectron spectroscopy (XPS) measurements supported our model shown in Figure 1a. Photoelectron yield spectroscopy (PYS) measurements suggested effective filling of density of states up to −3.8 eV versus vacuum in our process. The n-type chemical doping demonstrated in air is a key enabler for the fabrication of advanced devices via solution processing. In addition, electron transfer from fructose and FMN sheds light on a new connection between electronic materials and biomolecules, in terms of energy storage, transfer, and conversion.

2. Results and Discussion

2.1. n-Type Chemical Doping in Aqueous Solutions

Optical absorption measurements were performed to verify ambient n-type doping of organic semiconductor thin films. The chemical structures of the employed materials are shown in Figure 1b. We employed a polymer with naphthalene-1,4:5,8-bis(dicarboximide) (NDI) and thiophene backbone with branched alkyl chains (PNDI(2HD)T). Polymer thin films were spin-coated on glass substrates and thermally annealed (see Experimental Section for details). The doping solution was prepared by dissolving 1 M fructose, 10 mM FMN, and 10 mM 1,3-dimesitylimidazolium chloride (dMesIM-Cl) in an alkaline buffer solution and adding 9vol% acetonitrile to promotes dopant diffusion. Chemical doping was performed by immersing the thin films in the doping solution in air at room temperature. The results of the absorption measurements are shown in Figure 1c. The undoped pristine PNDI(2HD)T thin film exhibited the lowest energy excitation peak at *ca.* 610 nm. After immersion in the doping solution, this peak was bleached, and other peaks at *ca.* 500 and 785 nm appeared. This result is consistent with successful n-type doping of polymeric semiconductors with NDI units forming polarons.[17,28,29] The conductivity of the thin film increased from below 10^{-9} S cm^{-1} to 4 × 10^{-4} S cm^{-1} by our process as shown later, which also supports successful n-type doping. When fructose or FMN were not dissolved in the doping solution, no spectral changes were observed (Figure 1d). These results show that the use of both fructose and FMN is necessary to achieve n-type doping in our process.

Electrode potential measurements were performed to clarify the roles of fructose and FMN (**Figure** 2a,b). Three solutions were used in this experiment: a fructose solution (pH 10.6), FMN solution (pH 10.9), and solution containing both fructose and FMN (pH 10.4). Measurements with the fructose solution showed a potential of −40 mV (versus Ag/AgCl). Although fructose is expected to show a redox potential more negative than −700 mV at elevated temperatures and basic conditions[30] through the PCET reaction $C_6H_{12}O_6 + 2OH^- \rightarrow C_6H_{12}O_7 + H_2O + 2e^-$, its slow reaction rate at room temperature limits the attainable reducing power. Consistently, the attainable doping level was found to depend on the solution pH, as discussed in Note S1 (Supporting Information). The slow reaction rate is partly due to the small proportion of the endiol form, which contributes to the reducing power. When only FMN is dissolved, the electrode potential was *ca.* −20 mV versus Ag/AgCl. In contrast, when both fructose and FMN were dissolved, a shallow electrode potential of −490 mV versus Ag/AgCl was observed. This phenomenon is explained by the redox mediator model, where FMN accepts electrons from fructose and then donates electrons to the target electrode. Thus, while the reaction rate was too low for a direct redox reaction between the electrode and fructose, FMN accelerated the redox reactions by serving as a redox mediator. Details of electron transfer kinetics is discussed in Note S2 (Supporting Information). In addition, the solution with both fructose and FMN showed a shallow electrode potential at least for a few hours, demonstrating balanced reducing power and stability in air. Combining the evaluation of PNDI(2HD)T energy level (Note S3, Supporting Information), the energy diagram for the electron transfer relay is shown in Figure 2c.

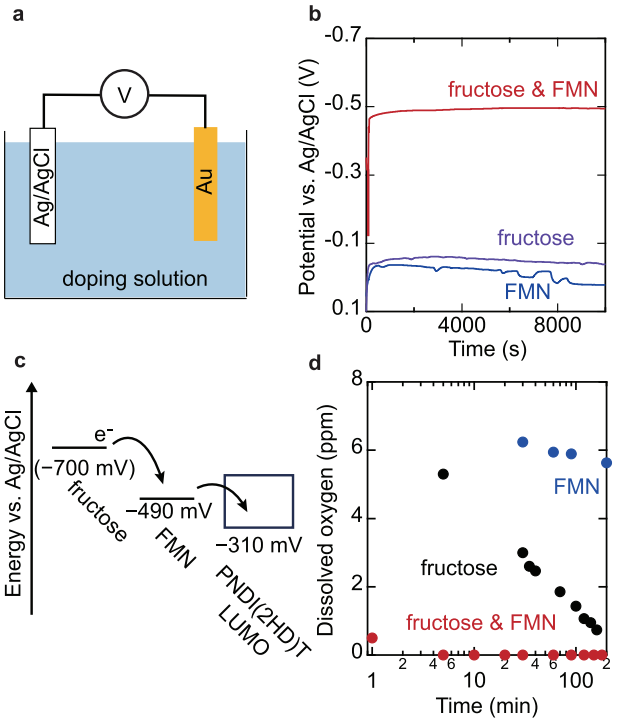

Figure 2. Roles of fructose and FMN. a) A schematic illustration of the electrode potential measurements in aqueous pH-buffer solutions. b) The results of electrode potential measurements. The compounds dissolved in solutions are denoted as legends. c) The energy diagram of our doping process. d) The change in amount of dissolved oxygen in the pH-buffer solutions by time. The dissolved compounds are denoted as legends.

During the doping process, oxygen in the aqueous doping solution is eliminated by redox reactions, which is supported by an evaluation of the concentration of dissolved oxygen (DO). DO was measured using a DO meter equipped with a membrane that selectively transports oxygen among redox-active materials. Note that most of the doping reaction is completed within one hour, based on the UV–Vis measurements shown in Note S4 (Supporting Information). Figure 2d shows the DO values measured in pH-buffer solutions containing fructose, FMN, or both. DO decreased slowly in the solution containing fructose, which is consistent with the slow redox kinetics of fructose. In contrast, the combination of FMN and fructose resulted in a sharp decrease in DO, with FMN serving as a redox mediator to accelerate the redox reaction rate. Thus, owing to the low solubility of oxygen in aqueous solutions and redox reactions with fructose and FMN, oxygen is present in our doping solution at very low concentrations and does not affect the doping efficiency.

Based on the above results, the effects of reactions with water and/or oxygen are suppressed in our doping method. Compared with the observed electrode potential of −490 mV versus Ag/AgCl in our system, the reduction potential of water is much more cathodic (*ca.* −790 mV versus Ag/AgCl[31]) at pH 10 and room temperature, where redox reactions with water may not give considerable effects. Note that the use of bulky hydrophobic ion is important for achieving doping at such a moderate potential.[21]

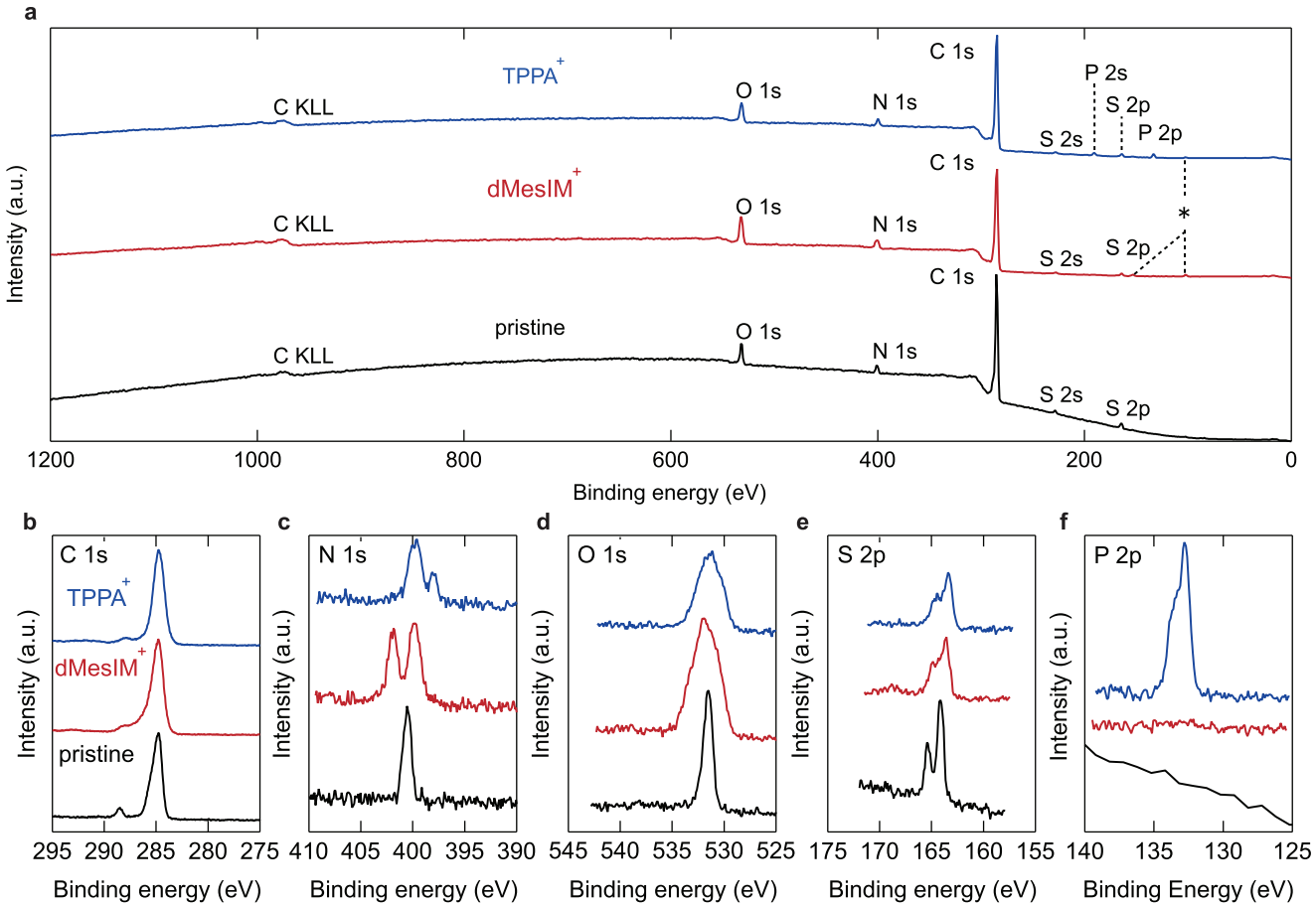

Figure 3. XPS spectra of doped thin films. a) XPS survey spectra of the pristine and doped PNDI(2HD)T thin films. The cations of the salts employed are denoted as legends for doped thin films. The peaks marked with asterisks are assigned to the Si atoms that can originate from the substrate. XPS narrow spectra of the pristine and doped PNDI(2HD)T thin films for b) C 1s, c) N 1s, d) O 1s, e) S 2p, and f) P 2p regions. The cations of the salts employed are denoted as legends for doped thin films.

Although oxygen can consume dopant materials, this does not limit the attainable doping levels during the process because of the low solubility of oxygen in water. Indeed, the solution with fructose and FMN showed negligible DO. Thus, the combined effects of solution pH, mediator-assisted use of fructose, and choice of dopant cation contributed to the achievement of ambient n-type chemical doping.

2.2. Identification of Introduced Molecular Cations

The dopant cations incorporated in the thin films were identified by X-ray photoelectron spectroscopy (XPS). In this experiment, doping solutions were prepared by adding salts of dMesIM-Cl or bis(triphenylphosphoranylidene)ammonium chloride (TPPA-Cl) to pH buffer solutions containing fructose and FMN. **Figure 3a** shows the XPS survey spectra of the PNDI(2HD)T thin films before and after the doping process. The pristine thin film exhibited peaks for carbon, nitrogen, oxygen, and sulfur atoms, which is consistent with the molecular structure of PNDI(2HD)T. When TPPA-Cl was dissolved in the doping solution, P 2s and P 2p peaks were observed, suggesting the successful introduction of $TPPA^+$ to the polymer thin film. The compositions of the doped thin films were further examined based on their narrow spectra (Figure 3b–f). When TPPA-Cl was used in the doping solution, new peaks appeared in the P 2p and N 1s regions. While undoped polymer showed an N 1s peak at 400.6 eV, the additional peak was observed at 398.0 eV, which is consistent with the binding energy expected for the nitrogen atom in $TPPA^+$. Note that the lower binding energy for the nitrogen atom in $TPPA^+$ compared to that of NDI is supported by our density functional theory (DFT) calculations (Note S5, Supporting Information), which indicate the negatively charged character of the nitrogen atom in $TPPA^+$. These results support the incorporation of $TPPA^+$ into the polymer thin film. When dMesIM-Cl was used in the doping process, a new peak was observed at 402.0 eV, which is consistent with the binding energy for positively charged nitrogen atoms in $dMesIM^+$, indicating the incorporation of $dMesIM^+$ in the thin film. The density of the incorporated cations was estimated by quantitative analysis of the XPS peaks. The ratios of the dopant/monomer unit were estimated to be 0.75 for $dMesIM^+$doping and 0.48 for $TPPA^+$-doping, respectively, based on the N 1s peak areas (Note S6, Supporting Information). These results suggest the

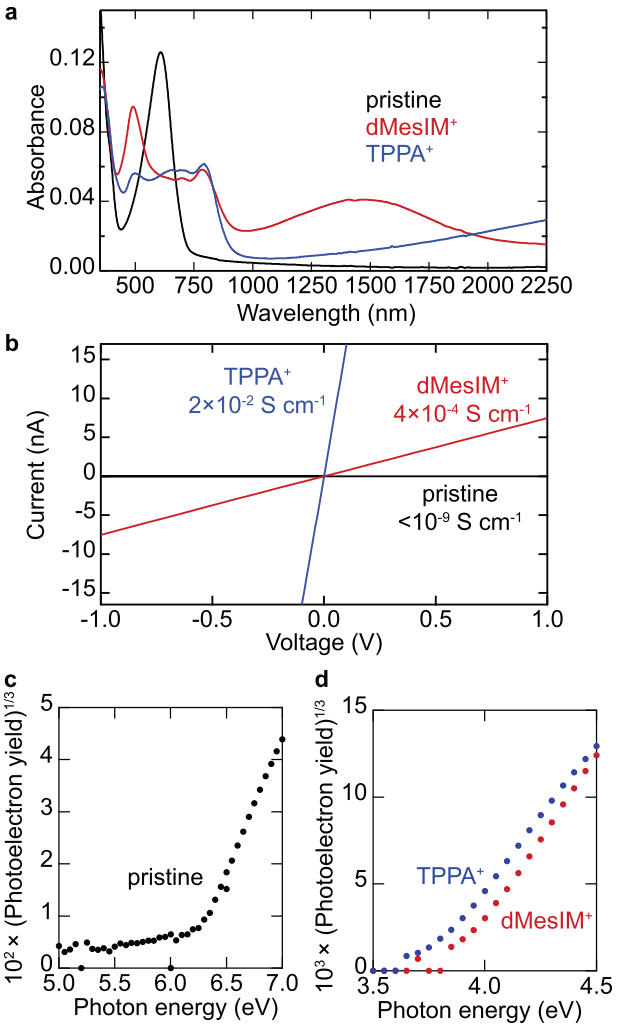

Figure 4. Electronic properties of doped thin films. Results of a) UV–Vis-NIR absorption, b) conductivity, and PYS measurements of c) the pristine and d) doped PNDI(2HD)T thin films. The dopant cations employed are denoted as legends. In PYS measurements, a deuterium (xenon) lamp was employed for the pristine (doped) thin films.

high doping levels of the polymer thin films achieved using our method.

The electronic properties of the dMesIM$^+$-doped and TPPA$^+$-doped thin films were further evaluated. In the UV–Vis–NIR spectra (**Figure** 4a), the dMesIM$^+$-doped PNDI(2HD)T thin film exhibited a near-infrared (NIR) absorption peak at approximately 1480 nm, which can be attributed to polaron absorption. For the TPPA$^+$-doped thin film, the NIR absorption peak shifted to a longer wavelength. Compared to the pristine thin film, the doped PNDI(2HD)T thin films showed significantly higher conductivities (Figure 4b). The TPPA$^+$-doped film exhibited a conductivity of 2× 10^{-2} S cm^{-1}, which was higher than that of the dMesIM$^+$-doped film. These results suggest that polarons are more delocalized in the TPPA$^+$-doped thin film than in the dMesIM$^+$-doped one, which may be attributed to differences in carrier concentrations, as discussed later. Photoelectron yield spectroscopy (PYS) measurements were performed to investigate changes in ionization potentials (IPs) upon doping (Figure 4c,d). In the PYS measurements, the wavelength of the incident UV light was swept while monitoring the photoelectron current and yield. The IP was determined as the threshold energy at which the cube root of the photoelectron yield begins to increase. The pristine PNDI(2HD)T film showed an IP of 6.26 eV, consistent with the deep-lying highest occupied molecular orbital (HOMO) of an n-type organic semiconductor. The doped thin films showed IPs of 3.73 eV for TPPA$^+$ doping and 3.85 eV for dMesIM$^+$ doping. These results are consistent with filling of the lowest unoccupied molecular orbital (LUMO) density of states and support the UV–Vis–NIR and conductivity measurements.

2.3. Stability of Doped State in Air at High Temperatures

The effects of the dopant cations on the stability of the doped thin films were evaluated based on the changes in conductivity over time. Thin films were stored at room temperature and 80% relative humidity, where dedoping by redox reactions with H_2O and O_2 is anticipated,[13] considering the shallow IPs of the doped polymers. As a reference, a well-studied n-type dopant, 4-(1,3-Dimethyl-2,3-dihydro-1H-benzimidazol-2-yl)-N,N-dimethylaniline (N-DMBI-H), was also used. N-DMBI-H doping was conducted in an N_2-purged glove box using an acetonitrile solution, where features of n-type doping were observed in UV–Vis measurements (Note S7, Supporting Information). In this case, N-DMBI$^+$ should be the dopant cation present in the polymer thin films.

The use of dMesIM$^+$ or TPPA$^+$ in our method resulted in superior ambient stability of the doped thin films compared to the case with N-DMBI-H doping (**Figure** 5a). While the initial conductivity measured was similar for N-DMBI$^+$- and dMesIM$^+$doped thin films, the N-DMBI$^+$-doped film showed a faster decay in the conductivity, which is consistent with our previous study.[17] The dMesIM$^+$-doped thin film exhibited an initial increase in conductivity for at least 4 h after air exposure. Changes in UV–Vis spectra are also shown in Note S8 (Supporting Information). This can be explained by the reported increase in conductivity with a decrease in the doping levels at very high doping levels close to one electron per monomer unit for NDI-based polymers.[17,32] This phenomenon also explains the differences in the UV–Vis–NIR spectra and conductivity measurements of TPPA$^+$- and dMesIM$^+$-doped thin films observed in Figure 3. For the tested three samples, the lifetimes of the doped state were evaluated based on the time required to observe a one-decade decrease in conductivity from the highest observed value (See Note S9, Supporting Information, for fitting). The lifetimes were 0.7 h, 1.7 h, and 28.7 h for N-DMBI$^+$-, TPPA$^+$, and dMesIM$^+$-doped thin films, respectively.

We also tested the thermal stability of the doped thin films in air (Figure 5b), which suggests the possibility of employing our n-type doped materials in applications including thermoelectric generators. The dMesIM$^+$-doped thin films were heated in air at 100 °C, and the conductivity was measured repeatedly at room temperature. The dMesIM$^+$-doped thin film exhibited a lifetime of 5 h, which is shorter than that of the test at room temperature. The results obtained at higher temperatures are presented in Note S10 (Supporting Information). When a PMMA thin film was spin-coated onto the doped PNDI(2HD)T thin film as an

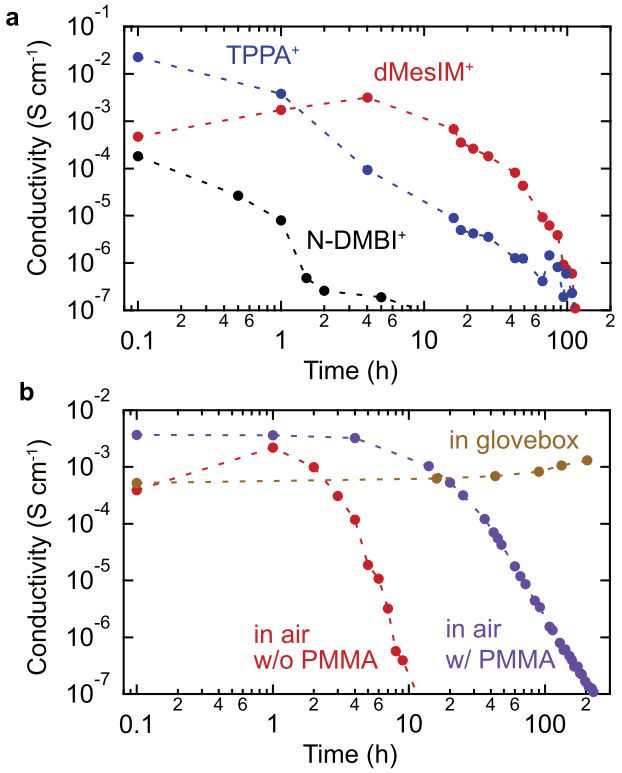

Figure 5. Stability of doped thin films in air. a) Changes in conductivity of doped PNDI(2HD)T thin films stored at room temperature and relative humidity of 80%. The dopant cations are denoted as legends. b) Changes in conductivity of $dMesIM^+$-doped PNDI(2HD)T thin films heated at 100 °C in air or in a glove box. Samples with or without a PMMA encapsulation layer were compared for the heating in air.

encapsulation layer, the lifetime increased to 25 h. When the heating process was conducted in a nitrogen-purged glove box and conductivity measurements were conducted in air, the thin film did not show a decrease in conductivity within 200 h, which supports the thermal stability of our thin film. Overall, the results suggest that the degradation of doped thin films at 100 °C in air occurs owing to accelerated reactions with O_2 and/or H_2O, which is dramatically suppressed by the choice of dopant cations and the use of facile thin-film encapsulation. The observed thermal stability in air was remarkable, considering the shallow IP of the doped thin films. Further exploration of dopant ions and polymers using our method will lead to shallow IP yet stable doped polymers, which is advantageous for applications such as thermoelectric generators and electron transport layers in photovoltaic cells. Considering the effective energy levels of the employed reducing agents, other types of polymers is expected to be compatible with our method (as partly demonstrated in Note S11, Supporting Information).

3. Conclusion

In this study, n-type chemical doping of a polymeric semiconductor was achieved using aqueous solutions in air, which was confirmed using absorption, XPS, conductivity, and PYS measurements. Fructose shows a slow redox reaction rate, which contributes to ambient stability, but limits its effective reducing capability. The use of the FMN redox mediator balances the redox reaction rate to achieve n-type doping. The $dMesIM^+$-doped PNDI(2HD)T thin film exhibited a conductivity of $> 10^{-3}$ S cm^{-1} and prolonged lifetime in air at room and elevated temperatures. Owing to the thermal stability of the material, facile thin-film encapsulation realized a lifetime of 25 h at 100 °C in air, which is remarkable considering the shallow IP of around 3.8 eV for the doped PNDI(2HD)T. These results suggest that our method will contribute to advanced organic devices using ambient p- and n-type doping in various applications, including thermoelectric generators and those requiring low-work-function yet stable electron transporting layers. Furthermore, the observed electron transfer between biomolecules and semiconductors opens new possibilities for achieving energy storage, transfer, and conversion.

4. Experimental Section

Sample Fabrication: EAGLE-XG (Corning) glass was employed for substrates. *o*-Dichlorobenzene (*o*DCB) was purchased from Tokyo Chemical Industry Co., Ltd. (TCI). PNDI(2HD)T, with an Mw of 268k, an Mn of 148k and a PDI of 1.81, was purchased from Ossila. The reducing agent D-fructose, the redox mediator FMN and the dopant salt dMesIM-Cl were purchased from TCI. TPPA-Cl was purchased from Fujifilm Wako. KOH, K_2HPO_4 and acetonitrile were purchased from Nacalai Tesque Corporation.

PNDI(2HD)T thin films were fabricated by spin-coating. The 1 wt% polymer solution in *o*DCB was preheated to 100 °C for dissolution. Spin-coating was conducted at 3000 rpm for 60 s. The thin films were heated to 200 °C under vacuum for solvent evaporation. The resulting PNDI(2HD)T thin film had a thickness of 33 nm.

Doping solutions were prepared by dissolving the chemicals in pH buffer. The pH buffer was prepared by dissolving about 80 mM of KOH and about 320 mM K_2HPO_4 in pure water. After dissolving 1 M fructose, 10 mM FMN-Na, 10 mM dMesIM-Cl or 0.1 mM TPPA-Cl in pH buffer, 9 vol% acetonitrile was added.

The Doping process was performed by immersing the PNDI(2HD)T thin films into the aqueous doping solutions for three hours.

Glass substrates were used for the UV-Vis absorption measurements. For electrical conductivity measurements, bottom contacts were prefabricated on glass substrates by thermal deposition of 3 nm Cr and 30 nm Au through shadow masks. The channel width and length were 2 mm and 170 μm, respectively. For XPS and PYS measurements, glass substrates were coated with 3 nm Cr and 30 nm Au by thermal deposition.

Measurements: UV–Vis was measured with V-670 spectrophotometer (JASCO). Electrical conductivity was measured with 2634B System SourceMeter (Keithley). DO was evaluated using a DO meter HI 2040-01 (HANNA instruments) based on the polarographic mechanism. XPS was performed using a KRATOS ULTRA 2 instrument with monochromatic Al Kα X-rays. PYS measurements were performed using the SUMITOMO PYS-202 instrument.

Supporting Information

Supporting Information is available from the Wiley Online Library or from the author.

Acknowledgements

This work was supported in part by JSPS KAKENHI grants (nos. JP23K23428, JP22H04959, JP23H05459, JP25H00898). This work was

supported in part by JST, CREST (no. JPMJCR21O3) and FOREST (no. JPMJFR236R). The DFT calculations in this study were performed on the Numerical Materials Simulator at NIMS.

Conflict of Interest

The authors declare no conflicts of interests.

Data Availability Statement

The data that support the findings of this study are available in the supplementary material of this article.

Keywords

chemical doping, electron transfer, organic semiconductor

Received: August 1, 2025
Revised: October 10, 2025
Published online: October 30, 2025

[1] G. Wang, F. S. Melkonyan, A. Facchetti, T. J. Marks, *Angew. Chem., Int. Ed.* **2019**, *58*, 4129.
[2] Z. Genene, W. Mammo, E. Wang, M. R. Andersson, *Adv. Mater.* **2019**, *31*, 1807275.
[3] Y. Lin, Y. Firdaus, M. I. Nugraha, F. Liu, S. Karuthedath, A.-H. Emwas, W. Zhang, A. Seitkhan, M. Neophytou, H. Faber, E. Yengel, I. McCulloch, L. Tsetseris, F. Laquai, T. D. Anthopoulos, *Adv. Sci.* **2020**, *7*, 1903419.
[4] Y. Lin, M. I. Nugraha, Y. Firdaus, A. D. Scaccabarozzi, F. Aniés, A.-H. Emwas, E. Yengel, X. Zheng, J. Liu, W. Wahyudi, E. Yarali, H. Faber, O. M. Bakr, L. Tsetseris, M. Heeney, T. D. Anthopoulos, *ACS Energy Lett.* **2020**, *5*, 3663.
[5] B. Russ, A. Glaudell, J. J. Urban, M. L. Chabinyc, R. A. Segalman, *Nat. Rev. Mater.* **2016**, *1*, 1.
[6] H.-I. Un, S. A. Gregory, S. K. Mohapatra, M. Xiong, E. Longhi, Y. Lu, S. Rigin, S. Jhulki, C.-Y. Yang, T. V. Timofeeva, J.-Y. Wang, S. K. Yee, S. Barlow, S. R. Marder, J. Pei, *Adv. Energy Mater.* **2019**, *9*, 1900817.
[7] S. N. Patel, A. M. Glaudell, K. A. Peterson, E. M. Thomas, K. A. O'Hara, E. Lim, M. L. Chabinyc, *Sci. Adv.* **2017**, *3*, e1700434.
[8] R. Kroon, J. D. Ryan, D. Kiefer, L. Yu, J. Hynynen, E. Olsson, C. Müller, *Adv. Funct. Mater.* **2017**, *27*, 1704183.
[9] Y. Kim, S. Chung, K. Cho, D. Harkin, W.-T. Hwang, D. Yoo, J.-K. Kim, W. Lee, Y. Song, H. Ahn, Y. Hong, H. Sirringhaus, K. Kang, T. Lee, *Adv. Mater.* **2019**, *31*, 1806697.
[10] B. Lussem, C.-M. Keum, D. Kasemann, B. Naab, Z. Bao, K. Leo, *Chem. Rev.* **2016**, *116*, 13714.
[11] Y. Kim, K. Broch, W. Lee, H. Ahn, J. Lee, D. Yoo, J. Kim, S. Chung, H. Sirringhaus, K. Kang, T. Lee, *Adv. Funct. Mater.* **2020**, *30*, 2000058.
[12] S.-J. Wang, M. Sawatzki, G. Darbandy, F. Talnack, J. Vahland, M. Malfois, A. Kloes, S. Mannsfeld, H. Kleemann, K. Leo, *Nature* **2022**, *606*, 700.
[13] C. G. Tang, M. C. Ang, K.-K. Choo, V. Keerthi, J.-K. Tan, M. N. Syafiqah, T. Kugler, J. H. Burroughes, R.-Q. Png, L.-L. Chua, P. K. H. Ho, *Nature* **2016**, *539*, 536.
[14] X. Lin, B. Wegner, K. M. Lee, M. A. Fusella, F. Zhang, K. Moudgil, B. P. Rand, S. Barlow, S. R. Marder, N. Koch, A. Kahn, *Nat. Mater.* **2017**, *16*, 1209.
[15] Y. Yamashita, J. Tsurumi, M. Ohno, R. Fujimoto, S. Kumagai, T. Kurosawa, T. Okamoto, J. Takeya, S. Watanabe, *Nature* **2019**, *572*, 634.
[16] S. Kohno, Y. Yamashita, N. Kasuya, T. Mikie, I. Osaka, K. Takimiya, J. Takeya, S. Watanabe, *Commun. Mater.* **2020**, *1*, 79.
[17] Y. Yamashita, S. Kohno, E. Longhi, S. Jhulki, S. Kumagai, S. Barlow, S. R. Marder, J. Takeya, S. Watanabe, *Commun. Mater.* **2024**, *5*, 79.
[18] M. Xiong, X.-Y. Deng, S.-Y. Tian, K.-K. Liu, Y.-H. Fang, J.-R. Wang, Y. Wang, G. Liu, J. Chen, D. R. Villalva, D. Baran, X. Gu, T. Lei, *Nat. Commun.* **2024**, *15*, 4972.
[19] J. Li, S. Deng, J. Hu, Y. Liu, *J. Mater. Chem. A* **2024**, *12*, 21434.
[20] W. Xiong, W. Tang, G. Zhang, Y. Yang, Y. Fan, K. Zhou, C. Zou, B. Zhao, D. Di, *Nature* **2024**, *633*, 344.
[21] M. Ishii, Y. Yamashita, S. Watanabe, K. Ariga, J. Takeya, *Nature* **2023**, *622*, 285.
[22] W. Zhao, J. Ding, Y. Zou, C. Di, D. Zhu, *Chem. Soc. Rev.* **2020**, *49*, 7210.
[23] J. Chen, W. Zhang, L. Wang, G. Yu, *Adv. Mater.* **2023**, *35*, 2210772.
[24] S. Griggs, A. Marks, H. Bristow, I. McCulloch, *J. Mater. Chem. C* **2021**, *9*, 8099.
[25] S. K. Mohapatra, S. R. Marder, S. Barlow, *Acc. Chem. Res.* **2022**, *55*, 319.
[26] H. Guo, C.-Y. Yang, X. Zhang, A. Motta, K. Feng, Y. Xia, Y. Shi, Z. Wu, K. Yang, J. Chen, Q. Liao, Y. Tang, H. Sun, H. Y. Woo, S. Fabiano, A. Facchetti, X. Guo, *Nature* **2021**, *599*, 67.
[27] S. V. Singh, O. Saxena, M. P. Singh, *J. Am. Chem. Soc.* **1970**, *92*, 537.
[28] D. Trefz, A. Ruff, R. Tkachov, M. Wieland, M. Goll, A. Kiriy, S. Ludwigs, *J. Phys. Chem. C* **2015**, *119*, 22760.
[29] X. Zhao, M. Alsufyani, J. Tian, Y. Lin, S. Y. Jeong, H. Y. Woo, Y. Yin, I. McCulloch, *Adv. Mater.* **2024**, *36*, 2412811.
[30] L. Saikhao, J. Setthayanond, T. Karpkird, T. Bechtold, P. Suwanruji, *J. Cleaner Prod.* **2018**, *197*, 106.
[31] S. G. Bratsch, *J. Phys. Chem. Ref. Data* **1989**, *18*, 1.
[32] Y. Yamashita, S. Jhulki, D. Bhardwaj, E. Longhi, S. Kumagai, S. Watanabe, S. Barlow, S. R. Marder, J. Takeya, *J. Mater. Chem. C* **2021**, *9*, 4105.